# EnviEye Air Pollution Monitoring System

TECHNICAL DOCUMENTATION
PATENT PENDING: #63250768

EnviEye Air Pollution Monitoring System
TECHNICAL DOCUMENTATION | PATENT PENDING #63250768

# Table of Contents

## Contents

# Introduction

Why MOS Gas Sensors?

Operating Principle

Gas Measurement Method

Gas Sensor Complex

# Why MOS Gas Sensors?

Metal oxide semiconductor (MOS) gas sensors employing tin oxide ($SnO_2$) as the primary sensing material show promise for ambient air pollution monitoring due to many advantageous features such as high sensitivity, fast response and recovery, versatile selectivity through operational temperature, capability for low-cost mass production, and applicability in small-scale mobile applications. MOS gas sensors make use of inexpensive sensing elements that use electrochemical reactions between target gases and a substrate electrode, producing a signal current in proportion to the gas concentration, which is reflected in the magnitude of sensor resistance.

The sensor technology has been shown to measure various volatile organic compounds, $NO_2$, CO, $CH_2$, and $H_2S$, with reasonable precision and accuracy. As a result, MOS sensor technology has been widely applied in automatic ventilation control systems, household applications, and recently also in toxic gas sensor devices. The present innovation seeks to employ MOS gas sensors for the measurement of concentrations of toluene (VOC), CO, NOx, $CO_2$, $CH_4$, $NH_3$, and/or $H_2S$ utilizing a sensor complex equipped with a temperature/humidity sensor and microcontroller to enable algorithmic correction for fluctuations in ambient temperature and humidity.

# Operating Principle

When semiconductor particles are heated in air at high temperatures, oxygen is adsorbed on the particle surface by capturing free electrons. The depletion layer thus formed is largely dependent on the radius of semiconductor particles used. If it is as small as conventionally used in gas sensors, the depletion can extend up to the whole area of each particle. If the size is far larger, on the other hand, depletion takes place conventionally on the periphery of each particle. The figure below shows how the energy band structure and the distribution of conduction electrons change with increasing the partial pressure of oxygen from zero (flat band state) to state I (regional depletion), II (border), and III (volume depletion). The adsorption equilibrium is attained by increasing the depletion layer thickness until the border is reached. Later, during volume depletion, however, the Fermi level is lowered by pkT ongoing from II to III while the layer thickness is kept constant.

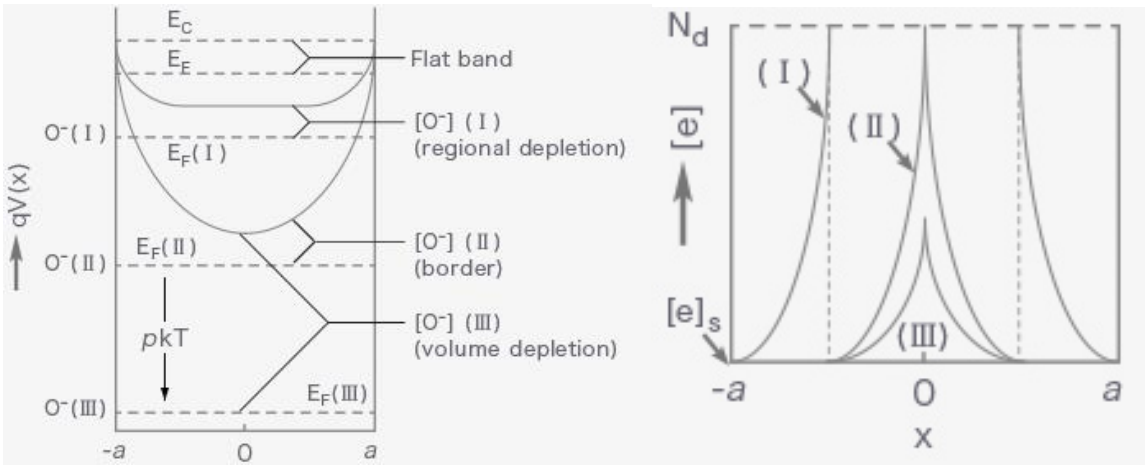


| | | |
|---|---|---|
| x | : | Distance in a radial direction |
| qV(x) | : | Potential energy |
| *a* | : | Particle radius |
| $[O^-]$ | : | Adsorbed oxygen concentration |
| $E_C$ | : | Conduction band energy |
| $E_F$ | : | Fermi level |
| *p*kT | : | Fermi level shift |

| | | |
|---|---|---|
| [e] | : | Electron concentration |
| $N_d$ | : | Donor density |

*Energy band structure (top) and distribution of conduction electrons (bottom) for a semiconductor particle as correlated with an increase in adsorbed oxygen concentration (Yamazoe et al., 2011)*

In this stage, two important equations are derived theoretically for a sensor device consisting of spherical particles, as follows.

$[e]_S=N_d \exp\{-(1/6)(a/L_D)^2-p\}$ ... (1) $R/R_0=N_d/[e]_S$ ... (2)

Here $[e]_S$ is the surface electron concentration of particles, and $L_D$ is the Debye length. R and $R_0$ are the sensor resistances at the steady-state and flat band state, respectively. When sensor materials are selected, $N_d$, *a*, $L_D$ and $R_0$ are fixed, while *p* is dependent on the actual gaseous conditions. As described, MOS-type gas sensors change resistance due to a change in adsorbed oxygen concentration. If this is used adequately, one can detect reducing gases like carbon monoxide. The adsorbed oxygen formed in clean air will be consumed on contact with carbon monoxide, the resulting decrease of R being used to estimate the concentration of carbon monoxide. The sensor recovers the original level of resistance when carbon monoxide is off. Such a detection mechanism is operative in tin dioxide-based gas sensors.

MOS gas sensor resistance ($R_s$) is calculated with a measured value of $V_{OUT}(V_{RL})$ by using the following formula:

$$R_s = \left(\frac{V_C}{V_{RL}} - 1\right) R_L$$

Where $V_C$ is the circuit voltage (in volts), $R_L$ is a load resistor (in ohms), and $V_{RL}$ is the voltage across the load resistor (in volts). One method of obtaining gas sample concentration algorithmically from the $R_s$ value is by conducting power regression on the sensitivity characteristics parameters of the sensor for different gasses provided by the manufacturer. Relating the sensor resistance ratio ($R_s/R_0$), where $R_0$ is sensor resistance in a sample of ambient "fresh" air at 20°C and 65% relative humidity to model standard test conditions, to the sample gas concentration yields the following formula:

$$C_{gs} = a\left(\frac{R_s}{R_0}\right)^b$$

Where $C_{gs}$ is the concentration of the gas sample (ppm) and [a, b] are coefficients specific to the gas chemistry. Employing this formula, a temperature/humidity dependency curve can be constructed, and the variability of the sensor resistance ratio over a chosen temperature and humidity range can be related. Note that inherent variability in $R_s$ response between sensors exists due to the manufacturing process, which makes for weak reproducibility. Therefore, a more accurate representation of sensor response is produced by applying $R_s/R_0$ in the extraction model, which is independent of variation among sensors in standard resistance readings. Modeling the necessary resistance ratio correction equation enables the generation of a sensor resistance correction factor, $K$, when combined with the response from an auxiliary temperature sensor. The $K$ value can be integrated into the gas concentration calculation equation based on a second-order polynomial model to yield corrected concentrations values using an adjusted exponential model as shown:

$$\mathrm{C_{gs}} = \mathrm{a}\left(\frac{\mathrm{R_S}}{\mathrm{R_0 K}}\right)^{\mathrm{b}}$$

Accurate gas concentration measurements can be obtained by applying this method for a MOS gas sensor's corroborating sensitivity curve.

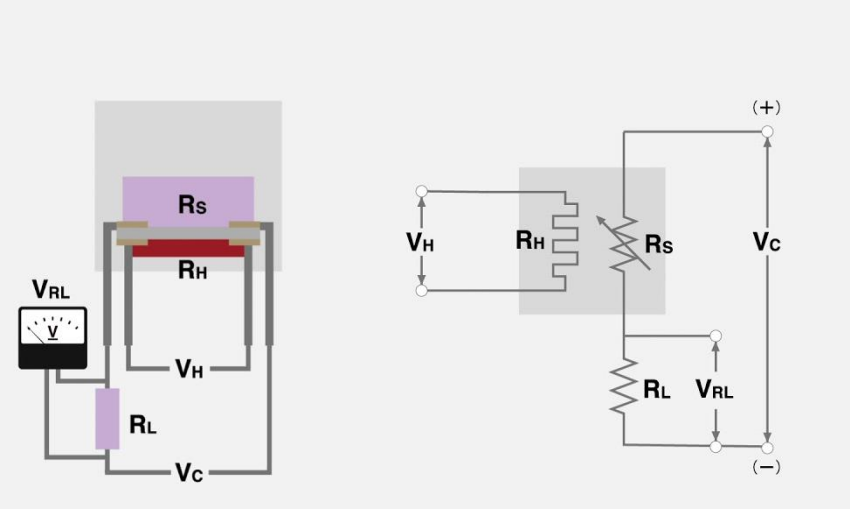


*MOS Gas Sensor Schematic (Figaro Engineering Inc., 2018)*

# Gas Selectivity

MOS gas sensors are limited by poor selectivity of gasses due to electron adsorption occurring due to interactions with non-target gasses. This poses a significant issue for MOS gas sensors use in ambient environments with the presence of multiple gas chemistries of unknown concentration.

To enhance selectivity, the proposed gas sensor complex hosts an array of tin oxide metal-oxide gas sensors to accomplish the direct measurement of $CO_2$, CO, and NOx with thermal selectivity to regulate sensor working temperature. Detection of trace concentrations of VOCs, $CH_4$, $NH_3$ and/or $H_2S$ is enabled by "cross selectivity correction". Based on the neural network machine learning algorithm proposed by Tayebi et al. in 2021, the employed method determines unique fingerprints of individual gases within a homogenous mixture by manipulating the multidimensional data from the three gas sensors and a temperature/humidity sensor. The program utilizes a trained hybrid regression/ANN algorithm to enable predictions under ambient conditions to yield self-calibrated concentration values that enable sensitive and selective gas sensing.

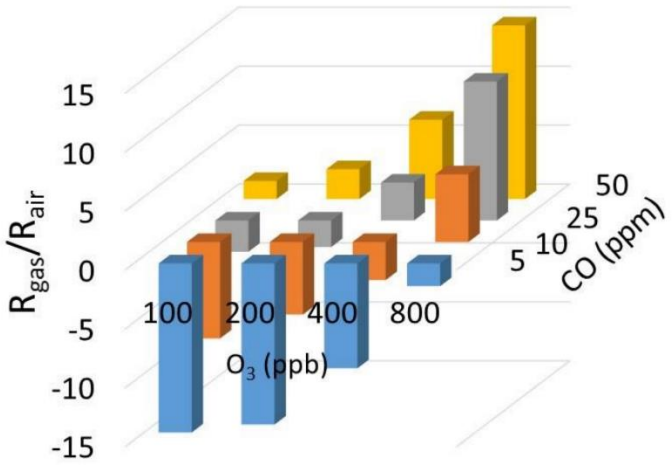


*Example 3D Histogram of $SnO_2$ Sensor Resistance Change at a Given $O_3$-CO Concentration Combination (Tayebi et al., 2021)*

Applying the procedure followed by Tayebi et al. for the $O_3$-CO experiment, similar machine learning training data sets were obtained for all the metal oxide sensors and at various operating temperatures and humidities under various target gas concentrations and combinations.

# Gas Sensor Complex

The proposed gas sensor complex applies the described gas concentration method and consists of an Arduino Nano for processing, a NodeMCU for WiFi connection, a Figaro TGS2600 gas sensor, a Figaro TGS2602 gas sensor, an MQ-135 gas sensor, and a DHT11 temperature/humidity sensor. The primary circuit is shown below with abstracted TGS260X, MQ-135, and DHT11 microcircuits.

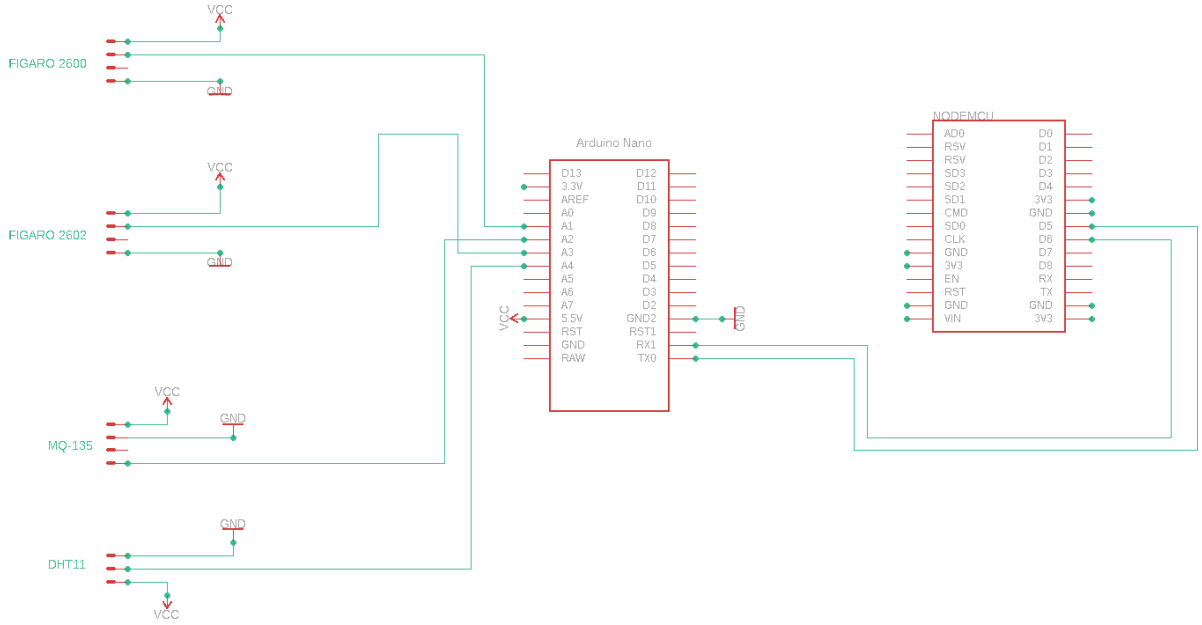


*Gas Sensor Complex Circuit*

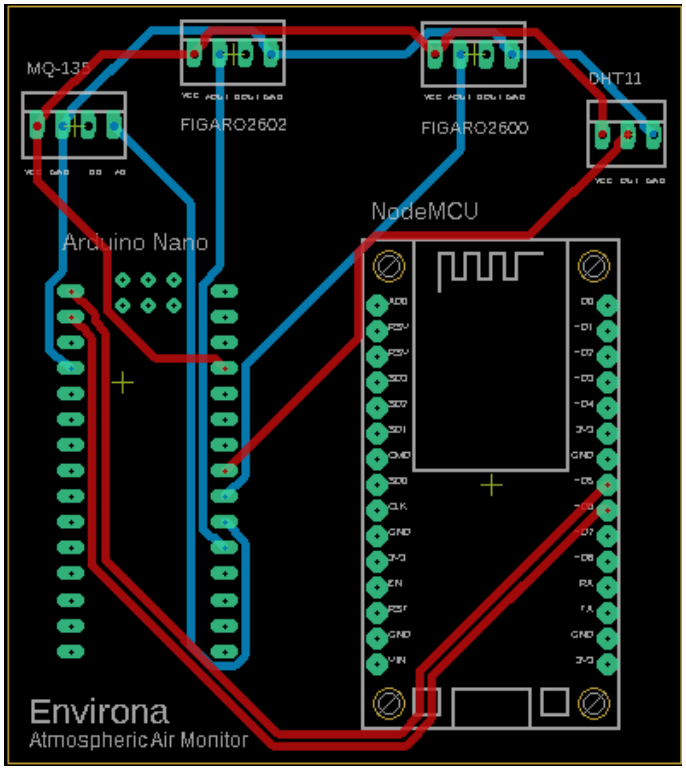


*Gas Sensor Complex PCB*

# Hardware

Figaro TGS260X Schematics and Calibration

MQ-135 Schematics and Calibration

DHT11 Schematics

Processors

# Figaro TGS260X Schematics

A custom microcircuit and PCB was designed for the TGS2600 and TGS2602 to mount the base model sensor. The schematics for the isolated sensor and microcircuit are shown below.

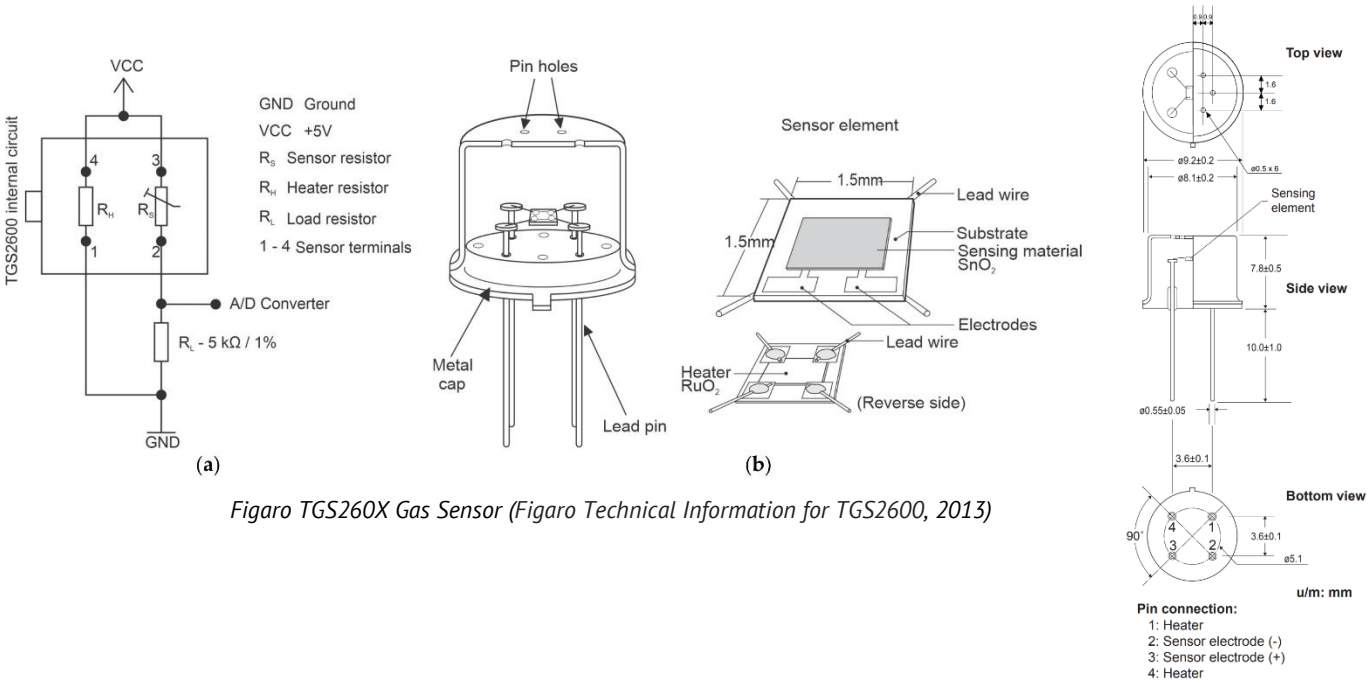


*Figaro TGS260X Gas Sensor (Figaro Technical Information for TGS2600, 2013)*

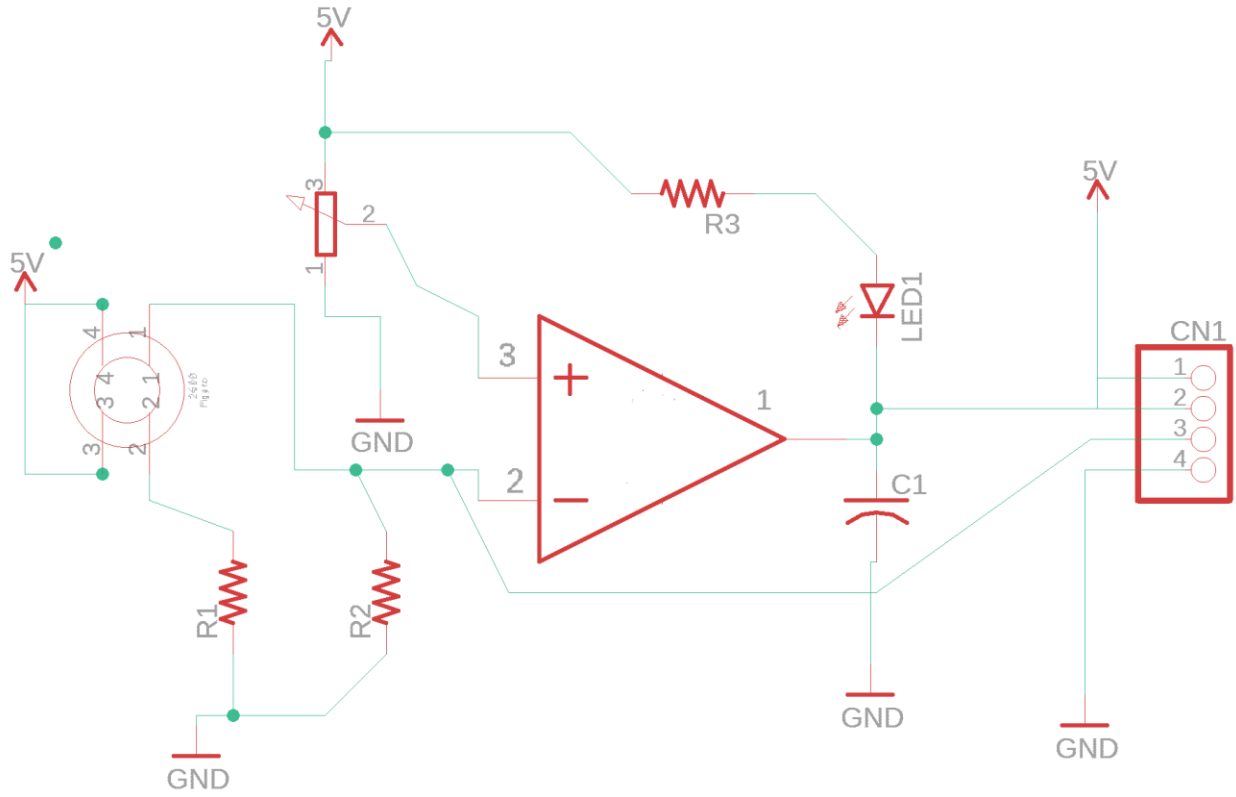


*Figaro TGS260X Microcircuit Custom Circuit Schematic*

# Figaro TGS260X Calibration

Figaro TGS260X calibration occurred under standard circuit conditions and standard test conditions. Sensors were allowed to reach equilibrium and given a conditioning period of 7 days prior to calibration. In a climate-controlled gas chamber, multi-point calibration occurred for each TGS2600 sensor in 11.1, 26.7, 34.9 PPM $H_2$ gas samples and for each TGS2602 sensor in 12.3, 27.4, and 36.3 PPM Ethanol gas samples.

| Typical detection range | | | 1 ~ 30ppm of $H_2$ | |
|---|---|---|---|---|
| Standard circuit conditions | Heater voltage | $V_H$ | 5.0±0.2V AC/DC | |
| | Circuit voltage | $V_C$ | 5.0±0.2V DC | Ps≤15mW |
| | Load resistance | $R_L$ | variable | 0.45kΩ min. |
| Electrical characteristics under standard test conditions | Heater resistance | $R_H$ | approx 83Ω at room temp. (typical) | |
| | Heater current | $I_H$ | 42±4mA | |
| | Heater power consumption | $P_H$ | 210mW | $V_H$=5.0V DC |
| | Sensor resistance | $R_S$ | 10kΩ ~ 90kΩ in air | |
| | Sensitivity (change ratio of Rs) | | 0.3~0.6 | $\frac{Rs\ (10ppm\ of\ H_2)}{Rs\ air}$ |
| Standard test conditions | Test gas conditions | | normal air at 20±2˚C, 65±5%RH | |
| | Circuit conditions | | $V_C$ = 5.0±0.01V DC<br>$V_H$ = 5.0±0.05V DC | |
| | Conditioning period before test | | 7 days | |

*Figaro TGS2600 Specifications (Figaro Engineering Inc., 2013)*

| Typical detection range | | | 1 ~ 30ppm of EtOH | |
|---|---|---|---|---|
| Standard circuit conditions | Heater voltage | $V_H$ | 5.0±0.2V AC/DC | |
| | Circuit voltage | $V_C$ | 5.0±0.2V DC | Ps≤15mW |
| | Load resistance | $R_L$ | variable | 0.45kΩ min. |
| Electrical characteristics under standard test conditions | Heater resistance | $R_H$ | approx 59Ω at room temp. (typical) | |
| | Heater current | $I_H$ | 56±5mA | |
| | Heater power consumption | $P_H$ | 280mW (typical) | |
| | Sensor resistance | $R_S$ | 10kΩ ~ 100kΩ in air | |
| | Sensitivity (change ratio of Rs) | | 0.08~0.5 | $\frac{Rs\ (10ppm\ of\ EtOH)}{Rs\ air}$ |
| Standard test conditions | Test gas conditions | | normal air at 20±2˚C, 65±5%RH | |
| | Circuit conditions | | $V_C$ = 5.0±0.01V DC<br>$V_H$ = 5.0±0.05V DC | |
| | Conditioning period before test | | 7 days | |

*Figaro TGS2602 Specifications (Figaro Engineering Inc., 2013)*

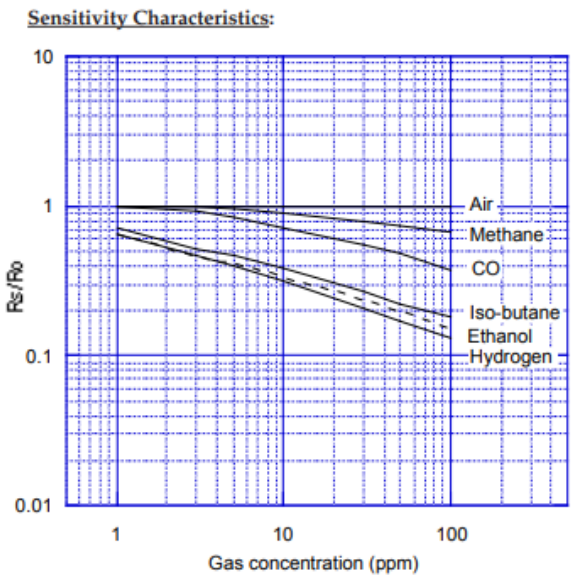


*Figaro TGS2600 Sensitivity (Figaro Engineering Inc., 2013)*

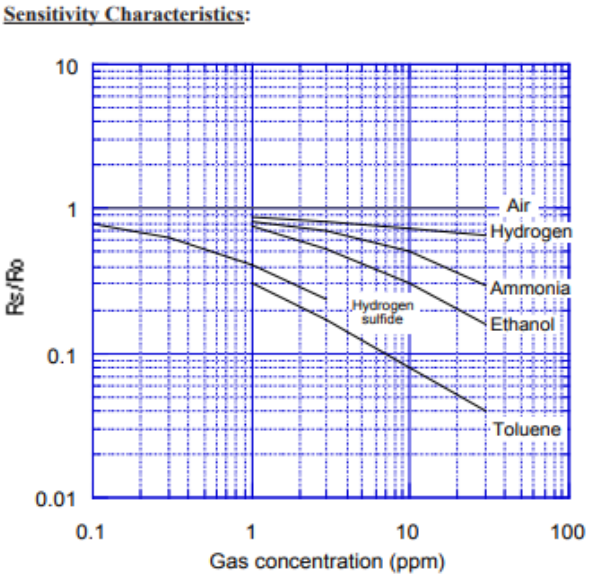


*Figaro TGS2602 Sensitivity (Figaro Engineering Inc., 2013)*

# MQ-135 Schematics

A custom microcircuit and PCB was designed for the MQ-135 to mount the base model sensor. The schematics for the isolated sensor and microcircuit are shown below.

| | Parts | Materials |
|---|---|---|
| 1 | Gas sensing layer | $SnO_2$ |
| 2 | Electrode | Au |
| 3 | Electrode line | Pt |
| 4 | Heater coil | Ni-Cr alloy |
| 5 | Tubular ceramic | $Al_2O_3$ |
| 6 | Anti-explosion network | Stainless steel gauze (SUS316 100-mesh) |
| 7 | Clamp ring | Copper plating Ni |
| 8 | Resin base | Bakelite |
| 9 | Tube Pin | Copper plating Ni |

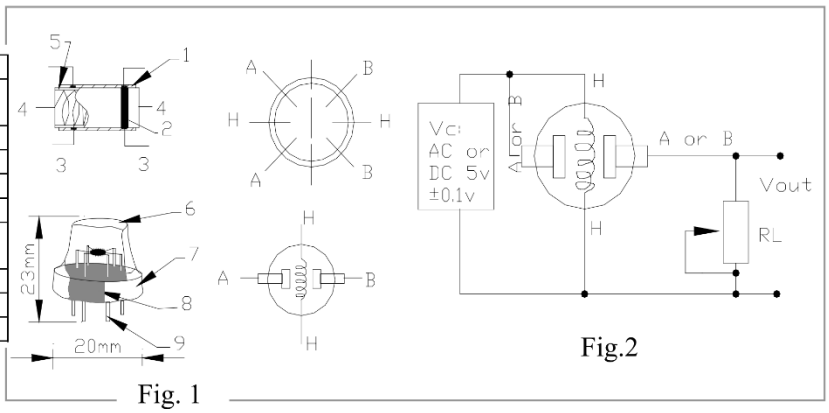


Fig. 1 Fig.2

*MQ-135 Physical Specifications (Technical Data: MQ-135 Gas Sensor, 2014)*

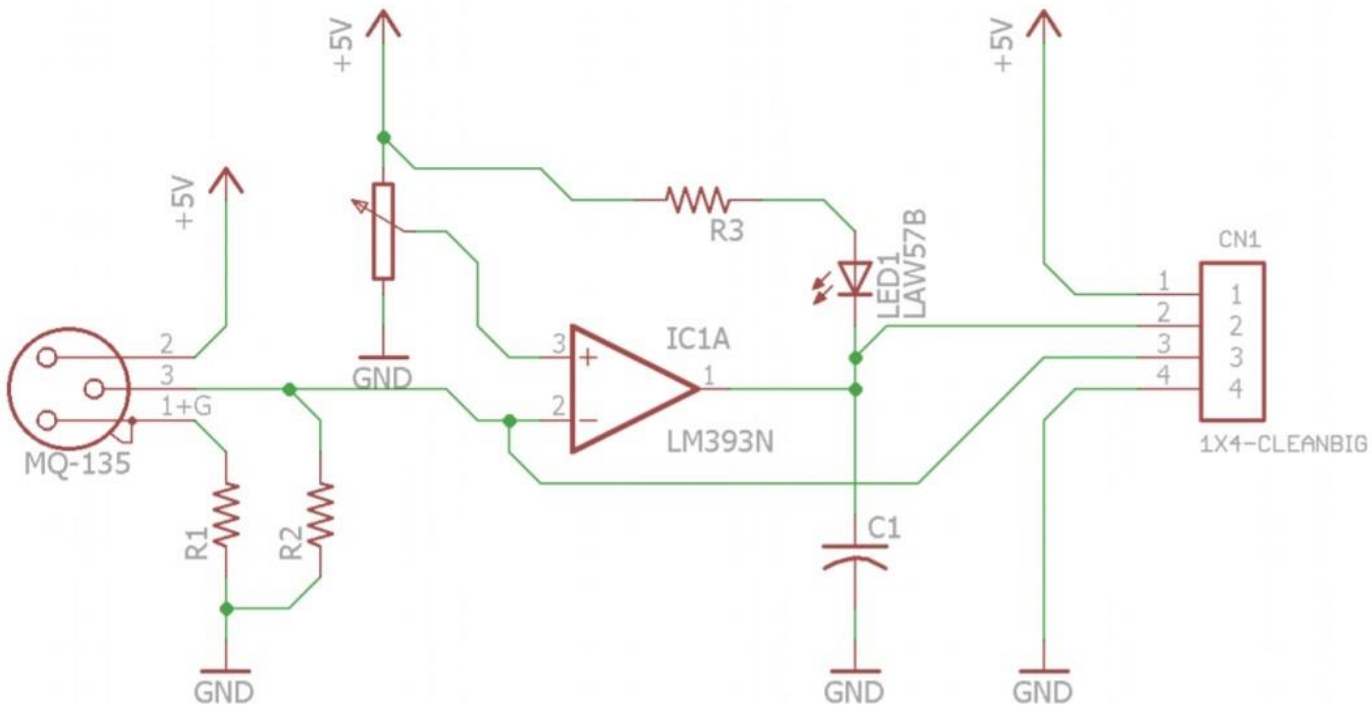


*MQ-135 Microcircuit Custom Circuit Schematic*

# MQ-135 Calibration

MQ-135 calibration occurred under standard circuit conditions and standard test conditions. Sensors were allowed to reach equilibrium and given a conditioning period of 24 hours prior to calibration. In a climate-controlled gas chamber, multipoint calibration occurred in 23.2, 53.4, and 107.1 PPM $NH_3$ gas samples.

A. Standard work condition

| Symbol | Parameter name | Technical condition | Remarks |
|---|---|---|---|
| Vc | Circuit voltage | 5V±0.1 | AC OR DC |
| $V_H$ | Heating voltage | 5V±0.1 | ACOR DC |
| $R_L$ | Load resistance | can adjust | |
| $R_H$ | Heater resistance | 33Ω±5% | Room Tem |
| $P_H$ | Heating consumption | less than 800mw | |

B. Environment condition

| Symbol | Parameter name | Technical condition | Remarks |
|---|---|---|---|
| Tao | Using Tem | -10 -45 | |
| Tas | Storage Tem | -20 -70 | |
| $R_H$ | Related humidity | less than 95%Rh | |
| $O_2$ | Oxygen concentration | 21%(standard condition)Oxygen concentration can affect sensitivity | minimum value is over 2% |

C. Sensitivity characteristic

| Symbol | Parameter name | Technical parameter | Ramark 2 |
|---|---|---|---|
| Rs | Sensing Resistance | 30KΩ-200KΩ (100ppm $NH_3$ ) | Detecting concentration scope 10ppm-300ppm $NH_3$ 10ppm-1000ppm Benzene 10ppm-300ppm Alcohol |
| α (200/50) $NH_3$ | Concentration Slope rate | ≤0.65 | |
| Standard Detecting Condition | Temp: 20 ±2 Vc:5V±0.1 Humidity: 65%±5% Vh: 5V±0.1 | | |
| Preheat time | Over 24 hour | | |

*MQ-135 Specifications (Technical Data: MQ-135 Gas Sensor, 2014)*

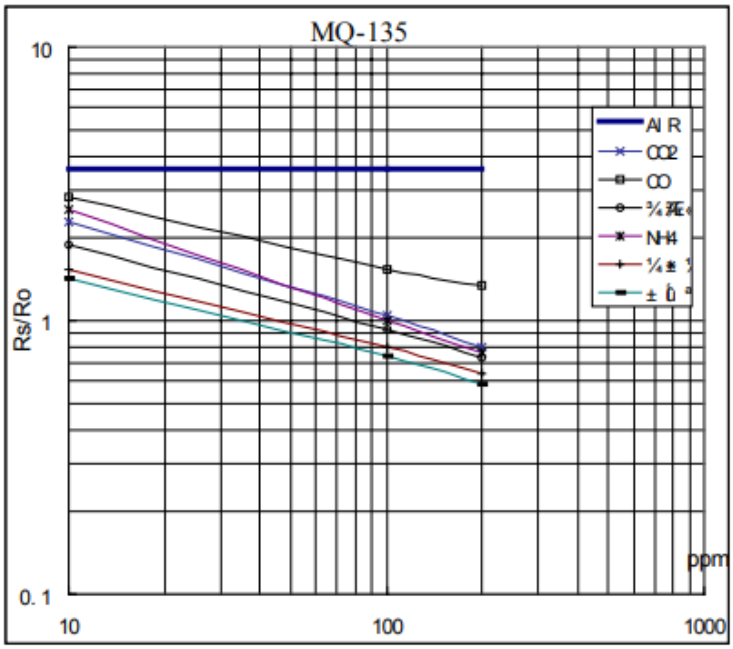


*MQ-135 Sensitivity (Technical Data: MQ-135 Gas Sensor, 2014)*

# DHT11 Schematics

DHT11 sensors provided the auxiliary temperature and humidity data necessary for the correction algorithm for the gas sensor complex. These sensors have been precalibrated by the manufacturer and have an accuracy of ±5%RH and ±2°C with a detection range of 20–90%RH and 0–50°C. Physical and circuit schematics are shown below.

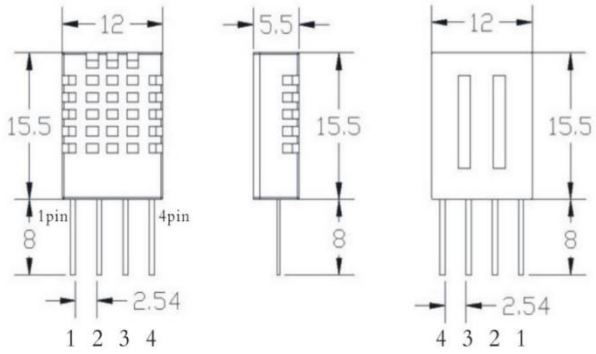


*DHT11 Physical Specifications (Aosong Guangzhou Electronics Co., Ltd., 2011)*

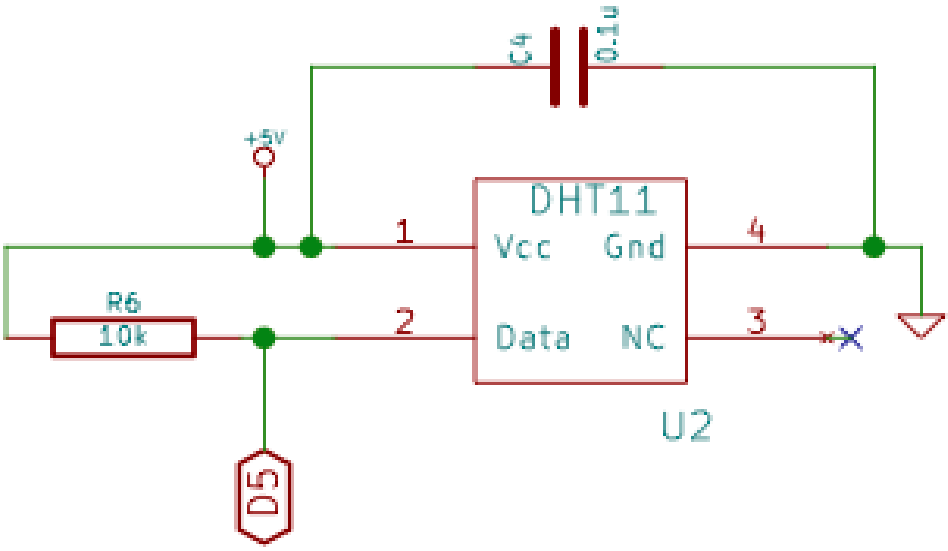


*DHT11 Transducer Module Circuit Schematic*

**Arduino Nano Microcontroller**

The Arduino Nano processes the incoming data from the sensor complex and integrates a correction algorithm to calculate the selected gas concentrations. A pinout diagram is shown below.

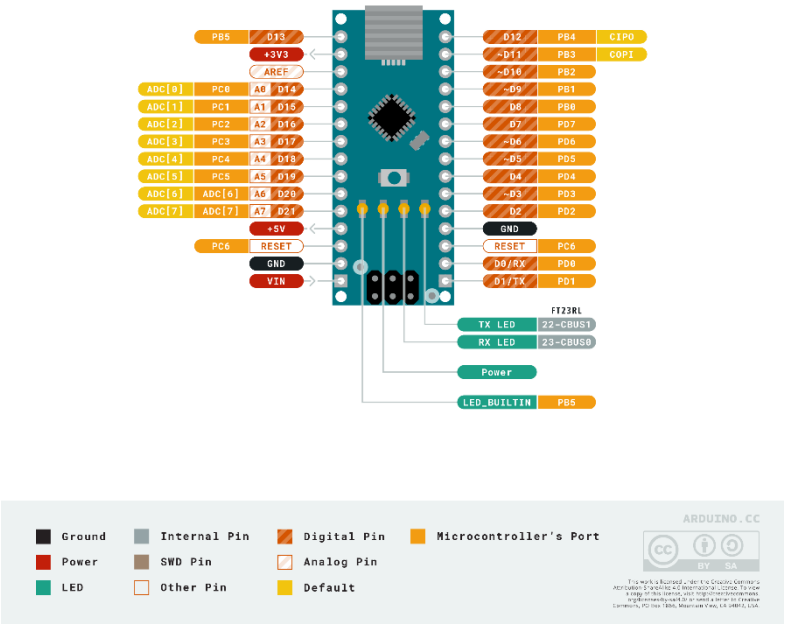


*Arduino Nano Microcontroller Pinout Diagram (Arduino Inc., 2021)*

**NodeMCU WiFi Module**

The NodeMCU ESP8226 module receives gas concentrations from the Arduino Nano and stores them temporarily. Employing the JSON library, the module utilizes a WiFi connection to the internet for live data uploads to a MATLAB ThingSpeak Channel. A pinout diagram is shown below.

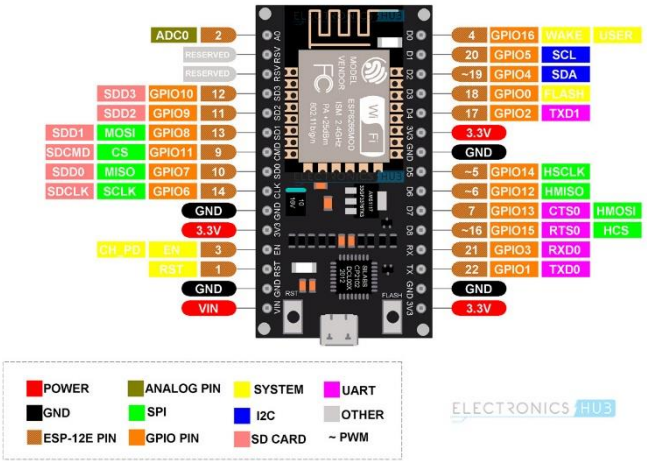


*NodeMCU WiFi Module Pinout Diagram (Electronics Hub, 2021)*

# Software

Sensor Program

Algorithmic Correction Method

Live Data Output

# Sensor Program

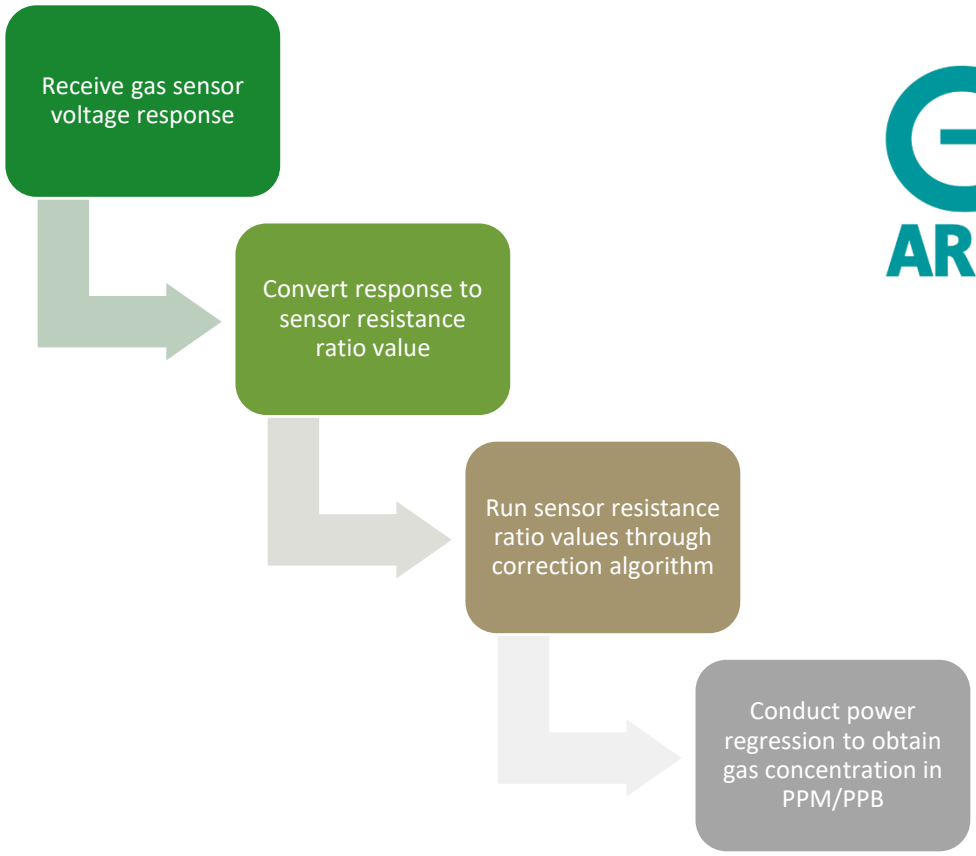


*Gas Concentration Extraction Code Logic (Arduino)*

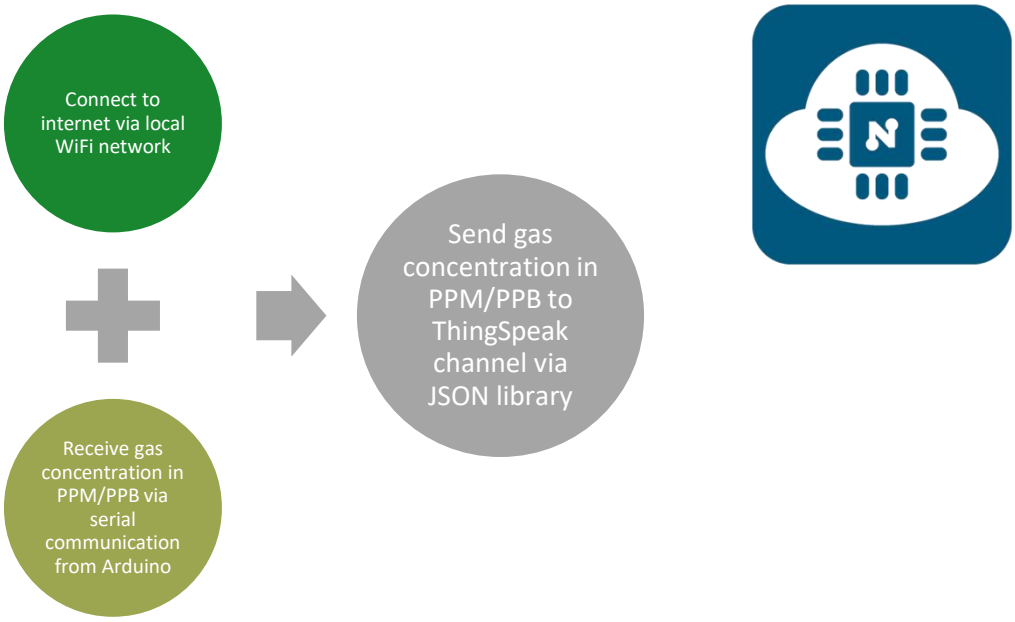


*Gas Concentration Data Feed Code Logic (NodeMCU)*

# Algorithmic Correction Method

To account for the MOS gas sensor's drift due to ambient temperature and relative humidity fluctuation, an algorithmic correction method was employed to produce corrected gas concentration values. A code logic diagram and schematic of the system mechanics are shown below.


*Correction Enabled Gas-Concentration Detector System Code Logic*

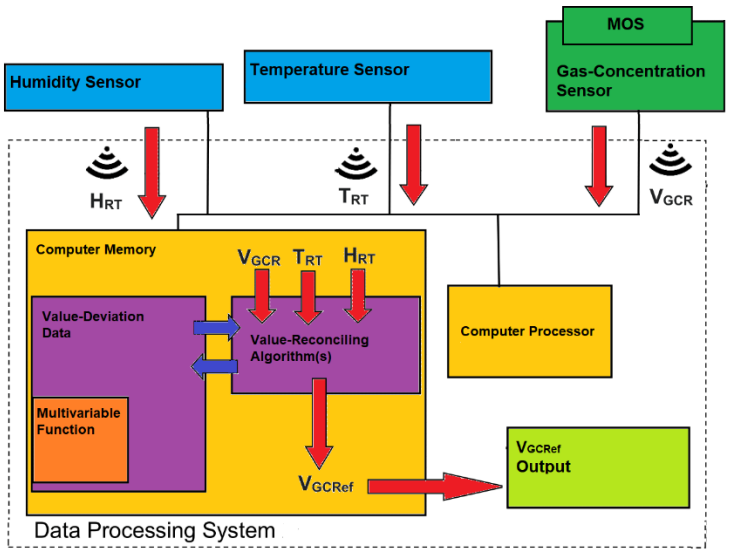


*Correction Enabled Gas-Concentration Detector System Schematic*

# Live Data Output

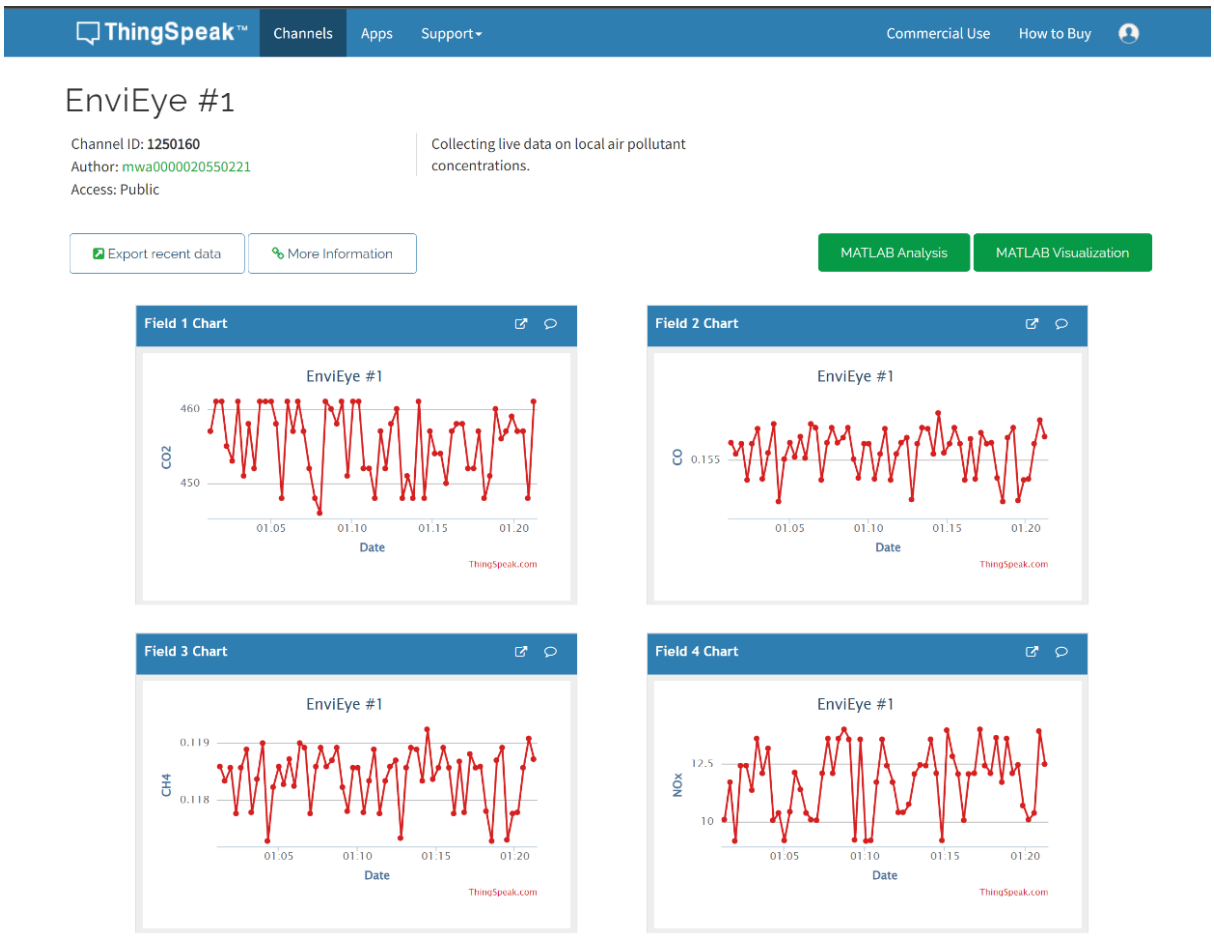


*MATLAB ThingSpeak Channel Sample Data from EnviEye Sensor #1*

*Air*

## Air Pollutant Information

| Pollutant | | Greenhouse Gas | Level | Long Term Adverse Health Effects |
|---|---|---|---|---|
| $CO_2$ | Carbon Dioxide | ✓ | 409.8 PPM | High blood pressure, lung diseases |
| CO | Carbon Monoxide | X | 9 PPM | Memory problems, difficulty concentrating, vision loss, hearing loss, and Parkinsonism |
| $CH_4$ | Methane | ✓ | 1.8 PPM | Development of epilepsy, pneumonia, claustrophobia, heart problems, memory loss, and depression |
| NOx | Nitrous Oxide | ✓ | 53 PPB | Vitamin B-12 deficiency, nerve damage, anemia, memory loss, birth defects, weakened immune system, lung disease, and asthma |
| $NH_3$ | Ammonia | X | 5 PPB | Chronic cough, asthma, lung fibrosis, eye membrane irritation, chronic respiratory irritation, and dermatitis |
| $H_2S$ | Hydrogen Sulfide | X | 0.3 PPM | Neurotoxicity, acute respiratory failure, convulsions, coma, brain and heart damage |
| Toluene | Volatile Organic Compound | X | 13 PPB | Chronic headaches, chronic nausea, liver and kidney damage, central nervous system damage, neurotoxicity, and cancer |

*Pollutant Concentration Typical Levels and Health Risks (USA EPA NAAQS Table, 2021; WHO Air Quality Guidelines for Europe, 2000)*

# Case Studies

Enclosure

MassDEP Testing

Nyanza Chemical Waste Dump

# Enclosure

The EnviEye enclosure is designed to be weatherproof and allow ample gas ventilation for accurate gas concentration measurements. PP GF30 (Polypropylene 30% glass fiber) was the selected 3D printing material because it is not only waterproof, but also resistant to aggressive environments, including high heat, UV, and chemicals.

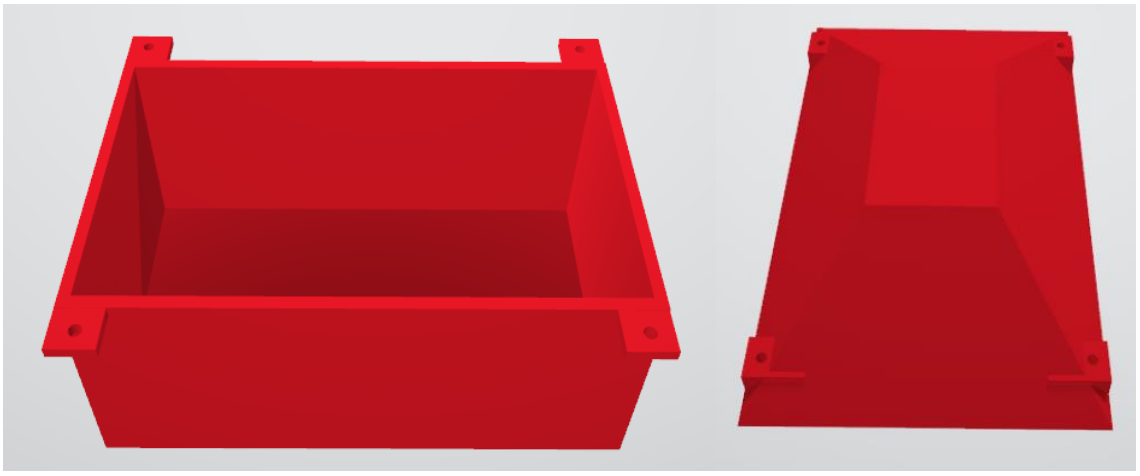

*EnviEye Enclosure 3D Schematics*

To verify whether the enclosure has adequate ventilation, a pulsed gas sample test was conducted. Utilizing an approach devised by Lello et al., the EnviEye Sensor was placed inside a gas chamber, exposed to ambient air, and then injected with ethylene gas to yield a 350 PPM $C_2H_4$ gas mix – the typical Figaro TGS260X upper test limit. Figaro TGS2600 sensor conductance and response time were then recorded and averaged for 10 trials in the gas chamber environment.

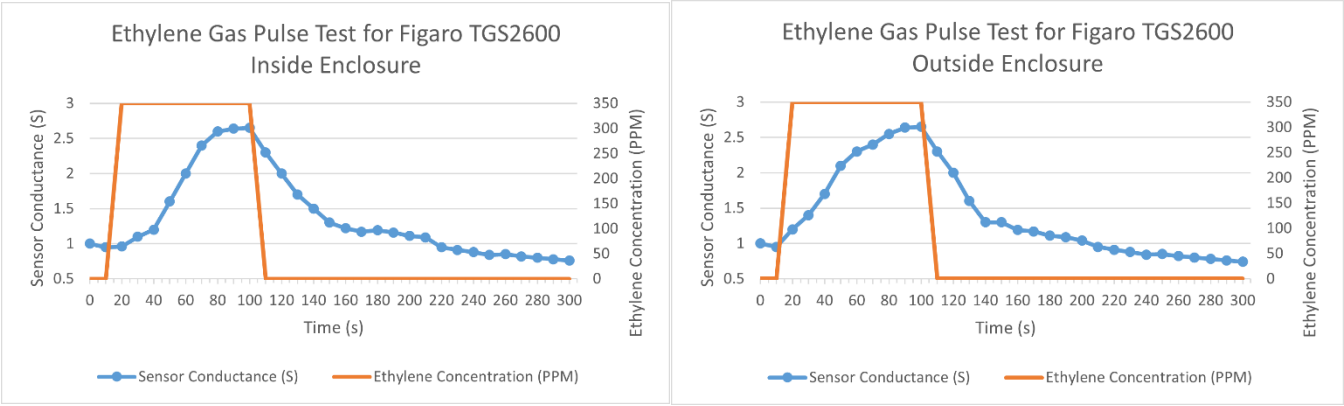


*Mean Response of Figaro TGS2600 Inside Enclosure versus Outside Enclosure to Ethylene Gas Pulse Test*

| Condition | Response Time (s) | Recovery Time (s) |
|---|---|---|
| Inside Enclosure | 23 ±5 | 117 ±5 |
| Outside Enclosure | 11 ±2 | 98 ±3 |

*Mean Response Time and Recovery Time Inside Enclosure versus Outside Enclosure Data Table*

The Figaro TGS2600 sensor inside the designed enclosure exhibits a comparable response and recovery time to the sensor outside the enclosure.

CO and NOx concentration measurement accuracy checks for the EnviEye sensor were conducted via collocation with a high-accuracy NDIR sensor hosted by the MassDEP in West Roxbury along Harrison Avenue. The NDIR sensor is ±20 PPB accurate for CO and ±5 PPB accurate for NOx. A thirty-day collocation period was chosen in the local ambient environment.

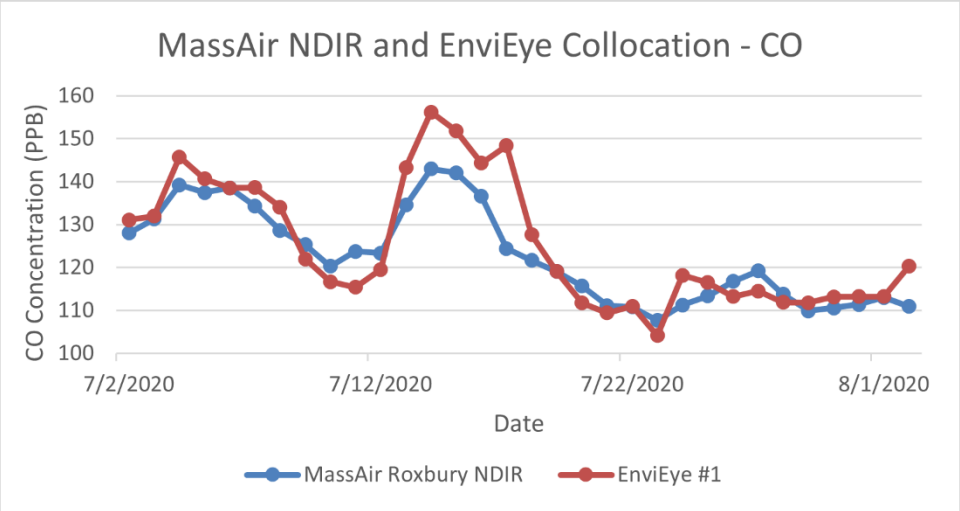


*MassDEP Roxbury Site NDIR Sensor vs. EnviEye Sensor #1 CO Accuracy Qualification 07/02/20 – 08/02//2020*

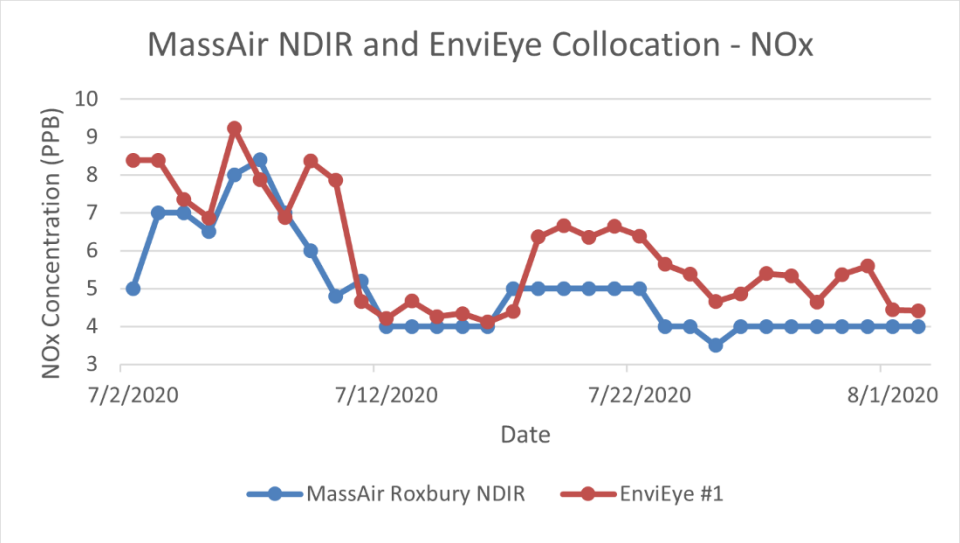


*MassDEP Roxbury Site NDIR Sensor vs. EnviEye Sensor #1 NOx Accuracy Qualification 07/02/20 – 08/02//2020*

| Sensor | Mean CO Concentration (PPB) | Mean Absolute Residual CO Concentration (PPB) | Mean NOx Concentration (PPB) | Mean Absolute Residual NOx Concentration (PPB) |
|---|---|---|---|---|
| MassAir NDIR | 122.702 | 4.911 | 4.950 | 1.099 |
| EnviEye #1 | 125.218 | | 5.936 | |

*MassDEP Roxbury Site NDIR Sensor vs. EnviEye Sensor #1 Accuracy Qualification Data Table*

The collected data demonstrates that the EnviEye Sensor's gas concentration measurements correlate to the MassDEP's NDIR Sensor with an accuracy of approximately ±5 PPB for CO and ±1 PPB for NOx.

# Nyanza Chemical Waste Dump

**Introduction**

In early 2020, EnviEye #1 detected higher than usual concentrations of toluene in the EPA Superfund Site Nyanza Chemical Waste Dump in Operable Unit II. Higher concentrations were notably observed near dense non-aqueous phase liquid (DNAPL) sites, a finding confirmed by previous EPA investigations corroborating VOC vaporization to DNAPL sites located under the waste dump.

**Health Risks**

Toluene is a VOC known to damage the human central nervous system, but the EPA has not found sufficient evidence of its carcinogenic effects. However, toluene is a precursor to benzene, another VOC with severe carcinogenic potential. As such, it is likely that the groundwater in toluene vaporization zones is also contaminated with benzene-containing DNAPL.

In addition, primary solvents purchased in 1970 by Nyanza Inc. included toluene and benzene derivatives, including nitrobenzene (30,250 lbs.), 2-nitrochlorobenzene (20,850 lbs.), 2-nitrotoluene (25,000 lbs.), and TCE (1,000 lbs.). This provides further evidence that DNAPL zones in the area are leaching toxic levels of toluene and benzene, posing a significant health risk to Ashland, MA residents living in the area.

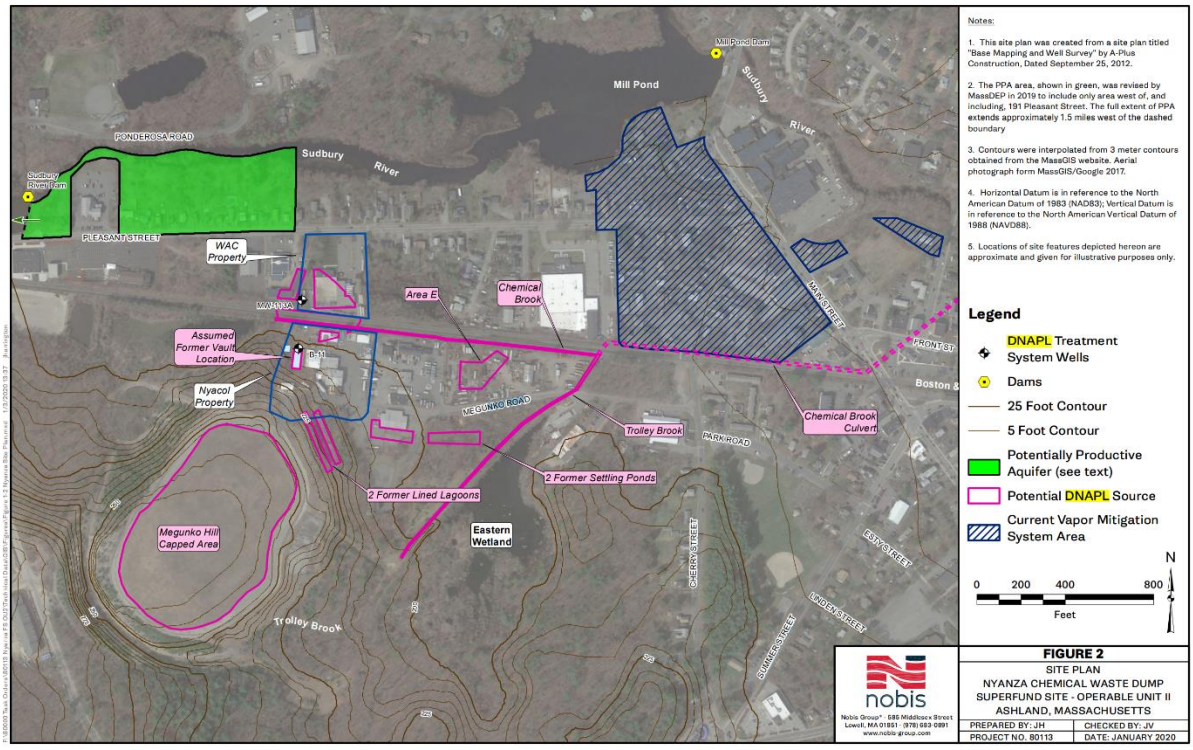


*Nyanza Chemical Waste Dump Operable Unit II Site Map with Highlighted Potential DNAPL Source Zone*

**Toluene Accuracy Qualification**

EnviEye Sensor #1 underwent rigorous toluene accuracy testing via collocation with the MassDEP's high-accuracy NDIR sensor located along Harrison Avenue in Roxbury. ANOVA statistical tests revealed that the correlation in an ambient environment for measured toluene concentrations between the MassAir Sensor and EnviEye Sensor #1 was significant. The EnviEye sensor was found to have an accuracy of ±10 PPB when compared to the NDIR sensing unit.

# Nyanza Chemical Waste Dump Cont.

**Location**

EnviEye Sensor #1 was located for a one-month period adjacent to the Chemical Brook along Megunko Road – the periphery of the potential DNAPL source zone highlighted in the map.

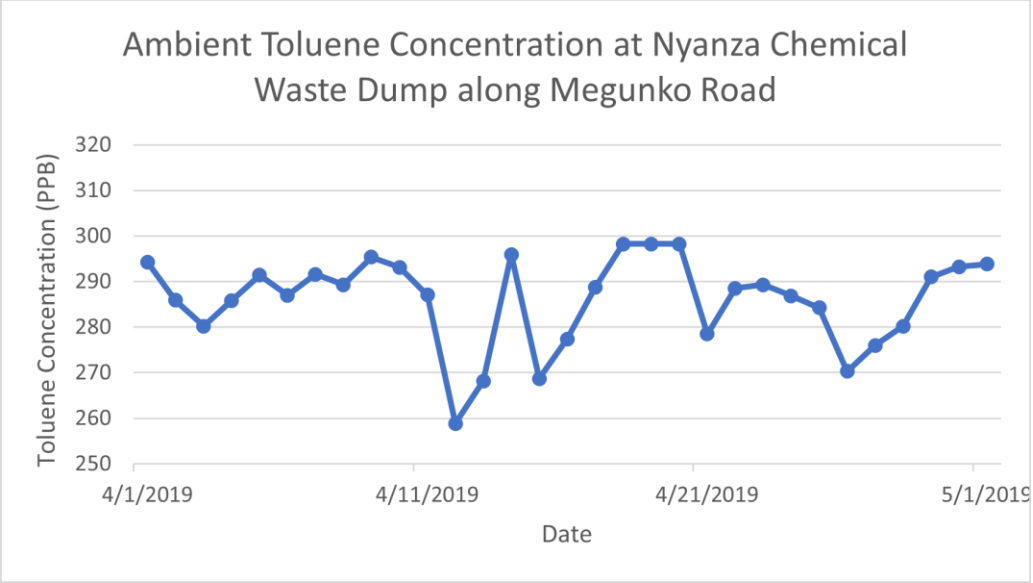


*EnviEye Sensor #1 Toluene Concentration Mean Daily Data Output 04/01/2019 – 05/01/2019*

**Data Interpretation**

The average mean daily toluene concentration measured at the site in a thirty-day time period was 285.965 PPB with a standard deviation of 9.822 PPB. The WHO Europe Air Quality Guidelines established worst-case exposure values relevant to a discussion of toluene's adverse health effects at a concentration of 38.57 PPB. Thus, toluene exposure by inhalation is a significant health risk in the Nyanza Chemical Waste Dump area.

**EPA Action**

Following the sample study, Environa began helping Ashland petition the EPA to develop a new cleanup plan to neutralize the toxic fume sources on Megunko Road. After months of attending community events and public forums, the community and EPA made a final decision on a remedy plan which considers factors like cost, disruption, effectiveness, and time to execute.

The selected remedy is intended to reduce the concentration of contaminants in groundwater to levels that will be protective of human health for exposure to indoor air, such that the existing vapor mitigation systems are no longer needed, and to minimize the need for controls to protect residents in outdoor environments. As of January 2020, the EPA has decided to launch a $20.5 million, 5-to-10-year initiative to drill into high DNAPL areas and excavate the contaminated groundwater.

# Sensor Drift Study

MOS in Ambient Environments

Multivariable Polynomial Modeling

CO Case Study

ANOVA Testing

CO Gas Selectivity

# MOS in Ambient Environments

Many drawbacks exist restricting the use of MOS gas sensors more widely in ambient environments for pollutant gas sensing. Those include frequently observed drift, poor quality due to reproducibility challenges, narrow dynamic range, and non-linear response. The main consequences of these drawbacks are poor accuracy and precision, especially in outdoor ambient applications where measurement conditions are highly variable.

Uncontrolled fluctuations of ambient temperature and relative humidity significantly reduce the accuracy of MOS gas sensors in field applications. As a result, temperature-induced drift is problematic to the use of MOS sensors in highly variable ambient environments. Therefore, quantifying the impact of temperature and relative humidity change followed by active correction is essential to improve the response accuracy of MOS sensors in ambient applications.

A study was conducted to characterize MOS gas sensor behavior as ambient temperature and relative humidity change simultaneously. Then, a novel method of combining an auxiliary temperature/relative humidity sensor with active algorithmic correction to improve sensor resistance drift was developed. The technique enables self-correction against ambient temperature and relative humidity fluctuations for MOS-based gas sensors. Utilizing this approach, the sensor performance was assessed with carbon monoxide gas samples over the temperature range from -10°C to 40°C and relative humidity intervals of 35%, 65%, and 95% for thirty randomly selected Figaro TGS2600 sensors.

The objective was to improve the accuracy of a tin oxide-based gas sensor by correcting for ambient temperature and relative humidity change. Two aspects of sensor performance were studied (1) sensor resistance variability correlation to temperature and relative humidity change, (2) improvement of sensor response accuracy by active algorithmic correction.

To do this, the sensor resistance change (Rs/Ro) was monitored across changing temperature and relative humidity conditions in a climate chamber. The selected temperature range was -10 to 40 degrees Celsius and the selected relative humidities were 35%, 65%, and 95%.

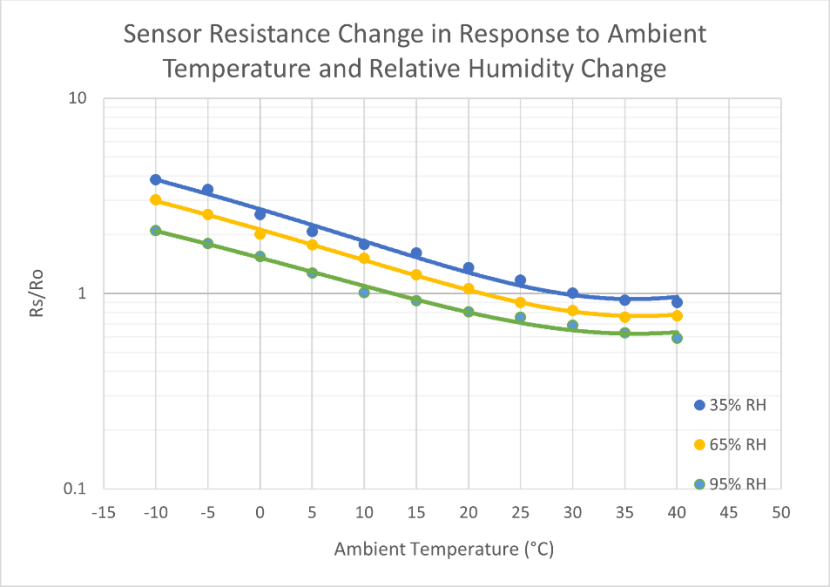


*Mean Sample Sensor Resistance Ratio Drift Over Variable Temperature and Relative Humidity Conditions with Second-Degree Polynomial Curve Trendlines.*

# Multivariable Polynomial Modeling

The symmetric nature of the Rs/Ro curves with vertical transformations suggests a limitation of the truncation of a multivariate Taylor series to only the second-order to model the relationship with temperature.

The second-order multivariable polynomial curve form is presented along with the mean coefficients in the table below.

$$K(T, R_H) = aT^2 + bR^2_H + cTR_H + dT + eR_H + f, \ \{(T, R_H) \mid -10 \leqslant T \leqslant 40, 35 < R_H \leqslant 95\}$$

Where $a$, $b$, $c$, $d$, $e$, and $f$ represent the coefficients that model the mean dependence of $R_s/R_0$ upon ambient temperature and relative humidity with a high coefficient of determination ($r^2 = 0.9873$).

| Coefficients | *a* | *b* | *c* | *d* | *e* | *f* |
|---|---|---|---|---|---|---|
| Mean curve | 0.00103 | $-3.101 \cdot 10^{-6}$ | $4.698 \cdot 10^{-4}$ | -0.105 | -0.0196 | 3.404 |

*Coefficients for the Best-Fitting Second-Order Multivariable Polynomial to Model Mean Sample Sensor Data*

To demonstrate the application of the model in a practical example and quantify its effectiveness in detecting CO concentration, measurements taken by the gas sensors in a 40 ppm CO gas mix were analyzed with and without the correction algorithm.

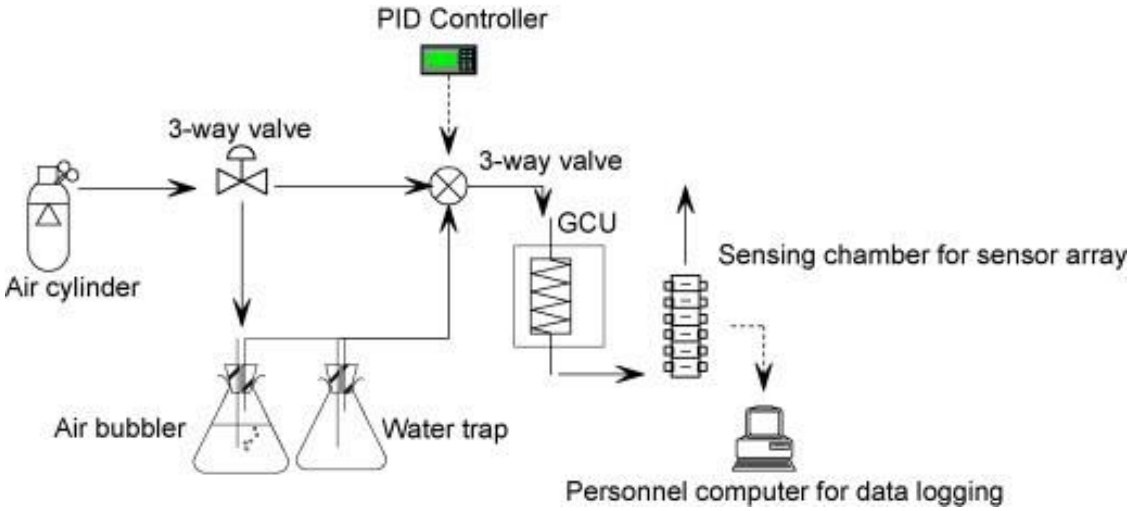


*CO Case Study Experimental Apparatus (Sohn et al., 2008)*

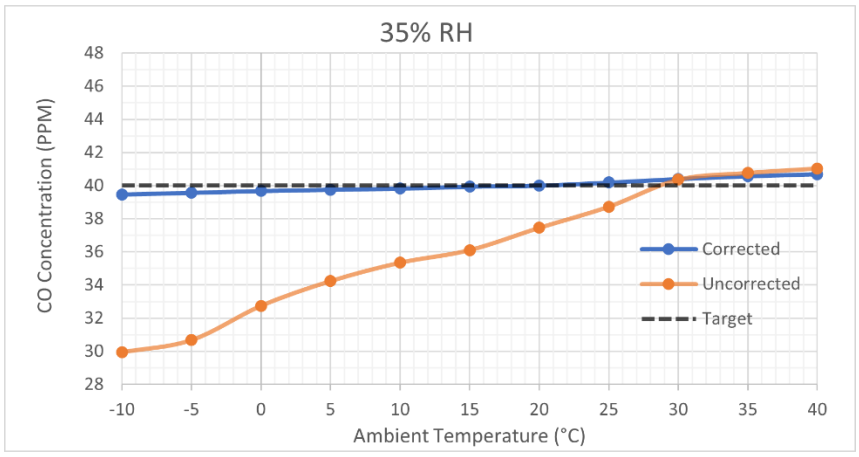


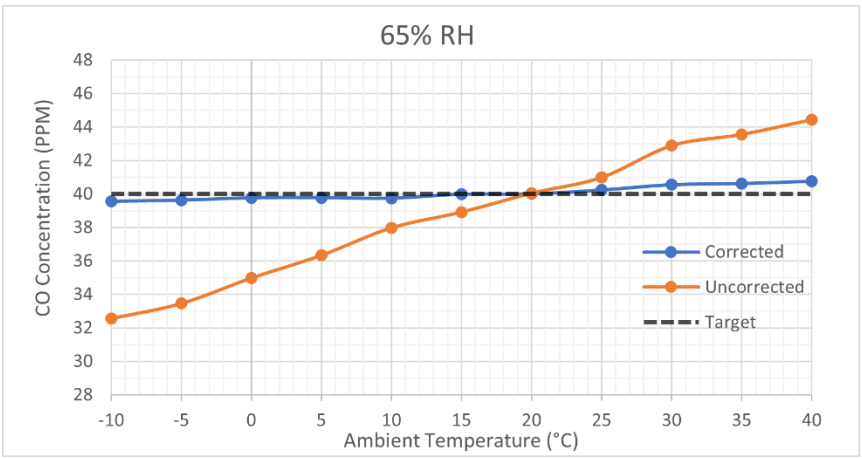

# CO Case Study Cont.

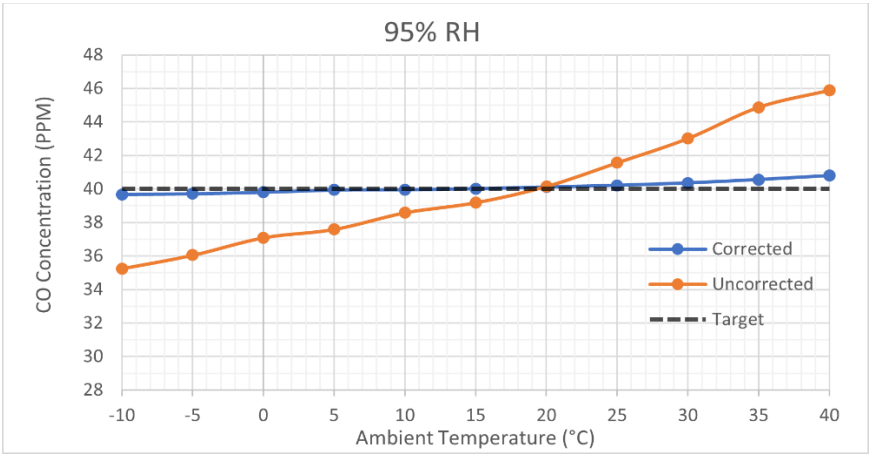


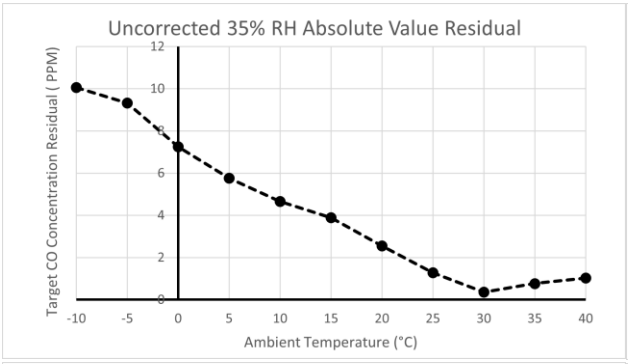


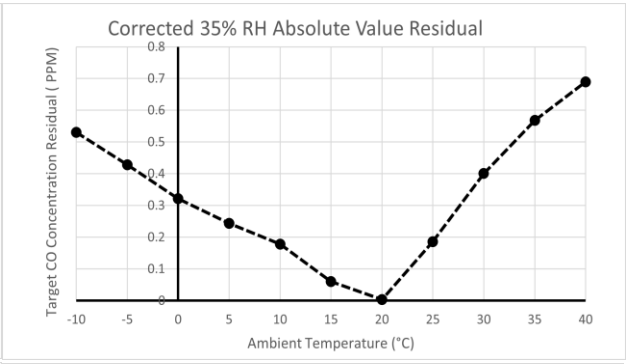


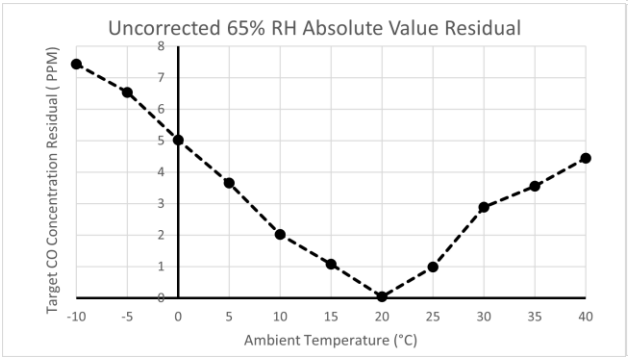


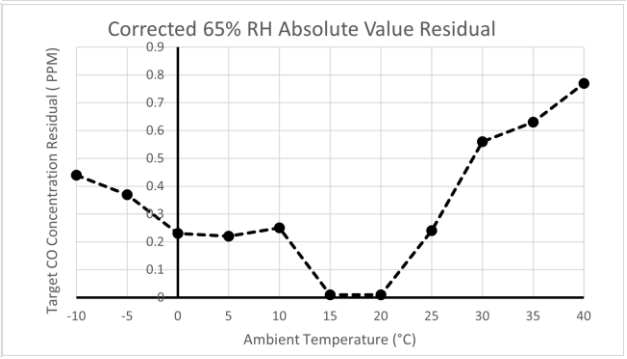


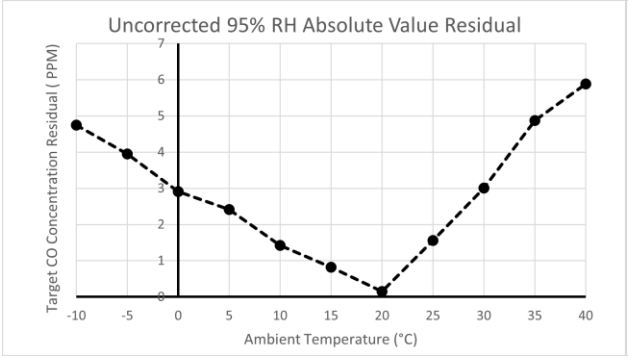


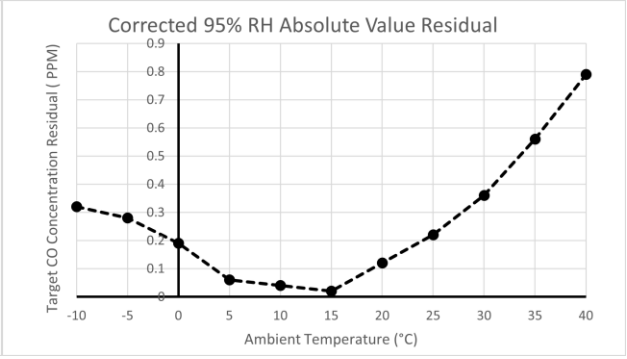


*Mean and Absolute Residual Sample CO Concentration at Various Relative Humidities for Corrected and Uncorrected Sensors*

# ANOVA Testing

To test the statistical significance of the correction method, an ANOVA test was conducted for the absolute value residuals of the corrected and uncorrected samples.

| Sensor Type | Parameter | 35% | 65% | 95% |
|---|---|---|---|---|
| Uncorrected | Mean | 0.328 | 0.339 | 0.269 |
| | Variance | 0.0471 | 0.059 | 0.056 |
| Corrected | Mean | 4.264 | 3.426 | 2.885 |
| | Variance | 12.038 | 5.455 | 3.341 |

*Absolute Residual Mean and Variance*

On average, the mean absolute residual is 11 times less for corrected samples than uncorrected samples, representing a substantial performance improvement.

| Relative Humidity | 35% | 65% | 95% |
|---|---|---|---|
| F-statistic | 22.153 | 19.014 | 14.099 |
| p-value | 0.000135 | 0.000303 | 0.00125 |

*ANOVA Testing Results*

ANOVA test results show that for all observed relative humidity conditions, F-statistics were higher than 1 at p-values lower than $\alpha = 0.05$. Thus, the variability between the corrected and uncorrected samples for absolute value residuals is significant.

# CO Gas Selectivity

The effect of interference gasses on the correction-enabled sensors' accuracy was investigated by applying the Carbon Monoxide Testing procedure to five separate gas mixes containing 40 ppm of CO and 5 ppm of either CO2, CH4, ethanol, LPG, or smoke. Each Figaro TGS2600 unit was operated at 250°C for sensor heater temperature-based gas selectivity of CO. Mean corrected sensor responses for all gas mixes are shown below.

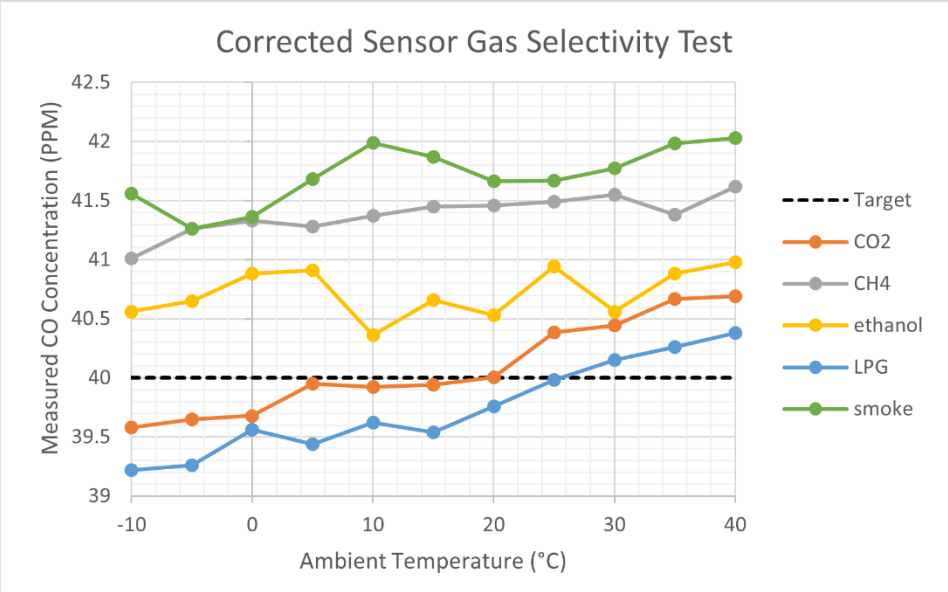


*Mean Corrected Gas sensor Response in Presence of Interference Gasses*

Despite the presence of interference gasses, the mean corrected gas sensor response maintains an accuracy of approximately ±2.0 ppm. The mean bias of LPG, CO2, and CH4 is minimized to values below ±1.0 ppm, but ethanol and smoke have a considerable effect on accuracy with a mean bias upwards of +1.0 ppm.

Sensors employing temperature-based selectivity and the correction algorithm also measured CO concentration with high accuracy despite the presence of potent interference gasses.

In selectivity testing, bias due to CH4, ethanol, and smoke (containing CO and trace VOCs) was likely higher because they are target gasses for SnO2 at operating temperatures closer to 250°C. Thus, when ambient temperature increased, the measured CO concentration increased as the gas sensors' sensing elements approached higher operating temperatures, and adsorption occurred with compounds other than CO. The ideal operating temperature for LPG and CO2 is lower than that of CO, thus the bias of these interference gasses is relatively low.

In any case, the selectivity tests demonstrate that controlling heater temperature through circuit manipulations affords a low-cost method of selectivity that warrants significant measurement accuracy when combined with the prescribed correction method. Such results confirm MOS gas sensor's potential for application in conventional field environments polluted by several gas types.

# Sensor Location

MassDEP Monitoring Network

EnviEye Monitoring Network

Harmful air pollutants surround our everyday lives. Sources of these chemicals include traffic, industrial units, chemical waste dumps, and even some agricultural practices. High concentrations of pollutants can be detrimental to health with short- and long-term consequences. Below is a map highlighting Primary Target Areas (PTAs) across Massachusetts.

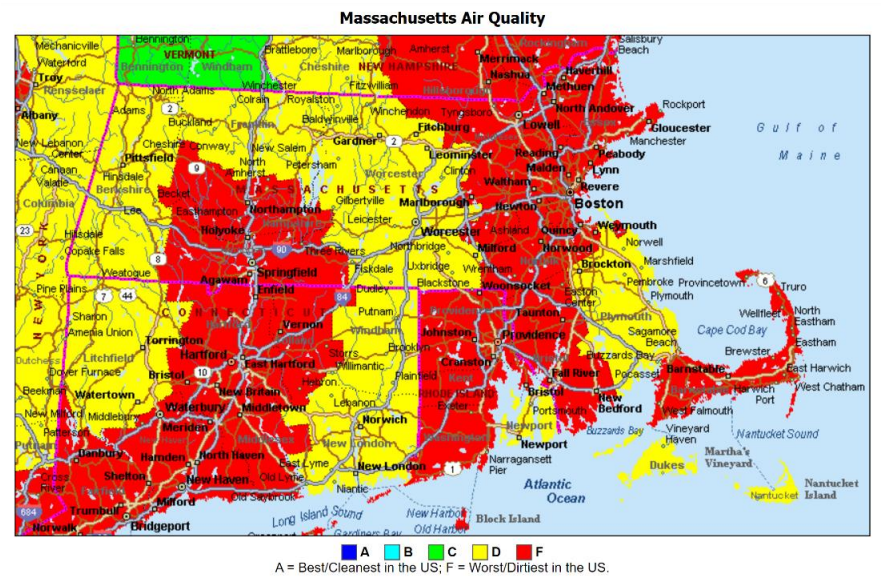


*Massachusetts Air Quality Map (Creative Method, 2021)*

However, the MassDEP's Air Monitoring Network reveals patterns in local detection undercoverage. Although air quality measurement operations are present in city areas, few operations are in the suburbs. The lack of data limits air pollution research and EPA action required to improve public health in high-risk areas.

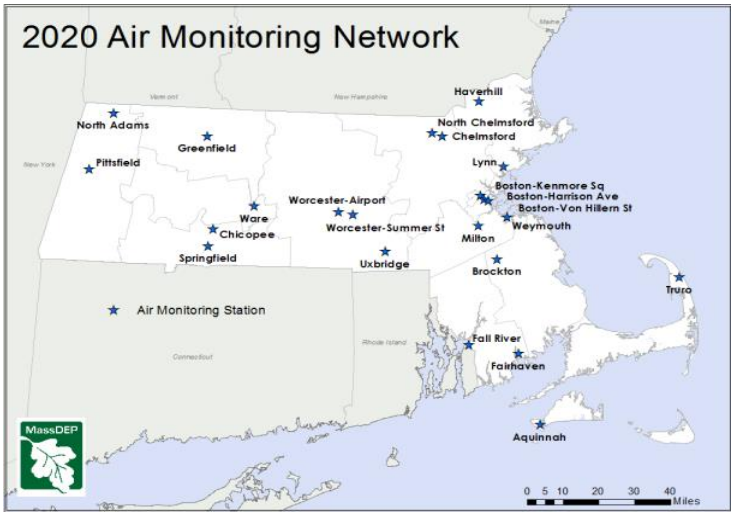


*MassDEP 2020 Air Monitoring Network (Massachusetts 2020 Air Monitoring Network Plan, 2020)*

# EnviEye Monitoring Network

With help from EPA, the EnviEye project gained permissions to deploy the sensor units in public libraries near high traffic areas, industrial/urban hotspots, and agricultural plots across Massachusetts. Below is a map of the 20 EnviEye units deployed by Environa Environmental.

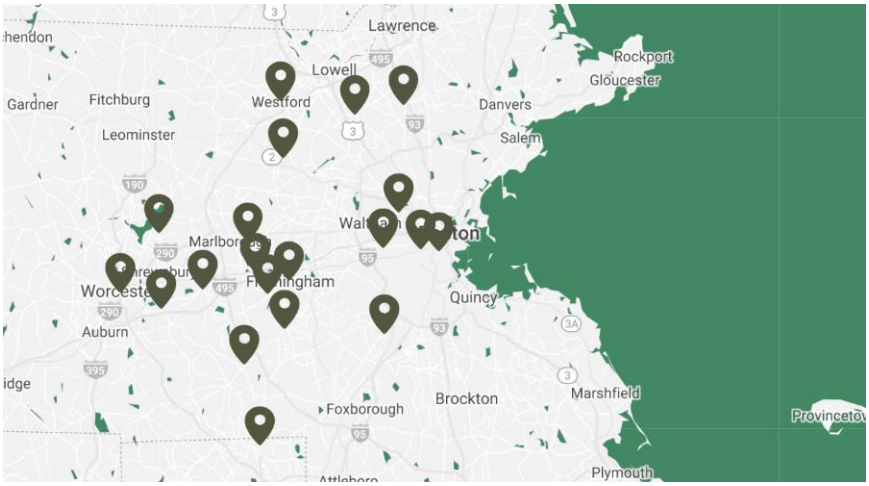


*EnviEye Air Pollution Monitoring Network*

| Sensor Number | Location | Status |
|---|---|---|
| 1 | 3 Blue Jay Ln, Ashland, MA 01721 | Active |
| 2 | 158 Union Ave, Framingham, MA 01702 | Inactive (August 7, 2021) |
| 3 | 1159 Harrison Ave, Roxbury, MA 02119 | Active |
| 4 | 151 Linden St, Boylston, MA 01505 | Active |
| 5 | 449 Boston Post Rd E, Marlborough, MA 01752 | Active |
| 6 | 16 School St, Milford, MA 01757 | Inactive (October 8, 2021) |
| 7 | 30 Turnpike Rd, Southborough, MA 01772 | Active |
| 8 | 777 Cass Ave, Woonsocket, RI 02895 | Active |
| 9 | 3 Salem St, Worcester, MA 01608 | Active |
| 10 | 361 Washington St, Brookline, MA 02445 | Active |
| 11 | 33 Walpole Street, Norwood, MA 02062 | Active |
| 12 | 21 Frederick Dr, Wilmington, MA 01887 | Active |
| 13 | 752 Washington St, Holliston, MA 01746 | Active |
| 14 | 55 West Main St, Westborough, MA 01581 | Active |
| 15 | 53 N. Main Street, North Grafton, MA, 01536 | Active |
| 16 | 15 Concord Rd, Billerica, MA 01821 | Active |
| 17 | 330 Homer St, Newton, MA 02459 | Active |
| 18 | 336 Concord Ave, Belmont, MA 02478 | Active |
| 19 | 486 Main St, Acton, MA 01720 | Active |
| 20 | 50 Main St, Westford, MA 01886 | Active |

*EnviEye Sensor Location Data Table*

The EnviEye network provides a resource for the American public, assisting with day-to-day decision-making concerning their health and the environment. The collected data is stored in an open-source ThingSpeak data repository to encourage local studies on ambient pollution and raise awareness for necessary EPA action in high health-risk areas.